Available online at www.sciencedirect.com
SCIENCE DIRECT®
Journal of Solid State Chemistry 179 (2006) 2690–2697
JOURNAL OF SOLID STATE CHEMISTRY
www.elsevier.com/locate/jssc

Crystal structures and phase stability in pseudobinary $CaAl_{2-x}Zn_x$

Karin Söderberg[a], Magnus Boström[b], Yoshiki Kubota[c], Takeshi Nishimatsu[d], Rainer Niewa[b], Ulrich Häussermann[a,*], Yuri Grin[b], Osamu Terasaki[a,*]

[a]*Department of Physical, Inorganic and Structural Chemistry, Arrhenius Laboratory, Stockholm University, SE-10691 Stockholm, Sweden*
[b]*Max-Planck-Institut für Chemische Physik fester Stoffe, Nöthnitzer Strasse 40, 01187 Dresden, Germany*
[c]*Department of Physical Science, Graduate School of Science, Osaka Prefecture University, Sakai, Osaka 590-0035, Japan*
[d]*Institute for Materials Science, Tohoku University, Sendai 980-8577, Japan*

Received 24 March 2006; received in revised form 10 May 2006; accepted 14 May 2006
Available online 26 May 2006

Abstract

Samples in the pseudobinary system $CaAl_{2-x}Zn_x$ ($0 \leqslant x \leqslant 2$) were synthesised from the elements. Three different structure types, the C15 and C36 Laves phase structures and the KHg_2 ($CeCu_2$) structure, were observed. The structures and homogeneity ranges of the underlying phases were investigated by electron microscopy and thermal analysis as well as X-ray powder diffraction. The stability ranges for the different structure types were found to be $0 \leqslant x \leqslant 0.18$, $0.28 \leqslant x \leqslant 0.68$ and $0.93 \leqslant x \leqslant 2$ for the C15, C36 and KHg_2 structure types, respectively.

Keywords: Intermetallic compounds; Laves phases; Pseudobinary systems phase diagrams; Structural stability

1. Introduction

Intermetallic compounds offer numerous possibilities to study the relationship between composition, crystal structure, chemical bonding and stability. Among the AB_2 systems, the most abundant are the Laves phases with more than 1400 representatives [1]. Their crystal structures are usually represented as close-packed arrangements of differently sized spheres maximising space filling. Accordingly, it has been discussed that the ratio of atomic radii, r_A/r_B, is an important factor for the overall stabilisation of Laves phases [2,3]. It has also been recognised that the overall valence electron concentration (VEC) plays a role in stabilising Laves phases [4]. Finally, the influence of the electron transfer between the A and B component, which is introduced by the electronegativity difference, has been addressed by Hafner [5]. However, due to the wide compositional variability of Laves phases it appears very difficult to establish general rules for their overall structural stability [6].

Laves phases crystallise predominately in three structure types: the cubic C15 or $MgCu_2$ type (polytype description 3C, space group $Fd\bar{3}m$), the hexagonal C14 or $MgZn_2$ type (2H, $P6_3/mmc$) and the C36 $MgNi_2$ type (4H, $P6_3/mmc$), which are called the primary Laves phase structures (cf. Fig. 1). The two components, A and B, form two interpenetrating nets (A and B net). The A nets in C15 and C14 correspond to cubic and hexagonal diamond, respectively. The C36 type is a periodic intergrowth of C15 and C14. Frequently, the crystal structures of Laves phases are also described in terms of layers with different stacking sequences. Sometimes periodic intergrowth produces ordered stackings beyond C15, C14, or C36, such as 6H, 16H and 21R. This polytype formation is observed, for example, in the systems $MgNi_{2-x}Cu_x$, $MgCu_{2-x}Zn_x$, and $MgZn_{2-x}Ag_x$ and has been analysed in electron microscopy studies [7–10].

Although many different systems with Laves structures have been reported, only a few s–p bonded representatives (that is compounds between main group metals) exist. This is probably because the rather large variations of size

*Corresponding authors.
E-mail addresses: ulrich.Haussermann@asu.edu (U. Häussermann), terasaki@struc.su.se (O. Terasaki).

0022-4596/$ - see front matter © 2006 Elsevier Inc. All rights reserved.
doi:10.1016/j.jssc.2006.05.018

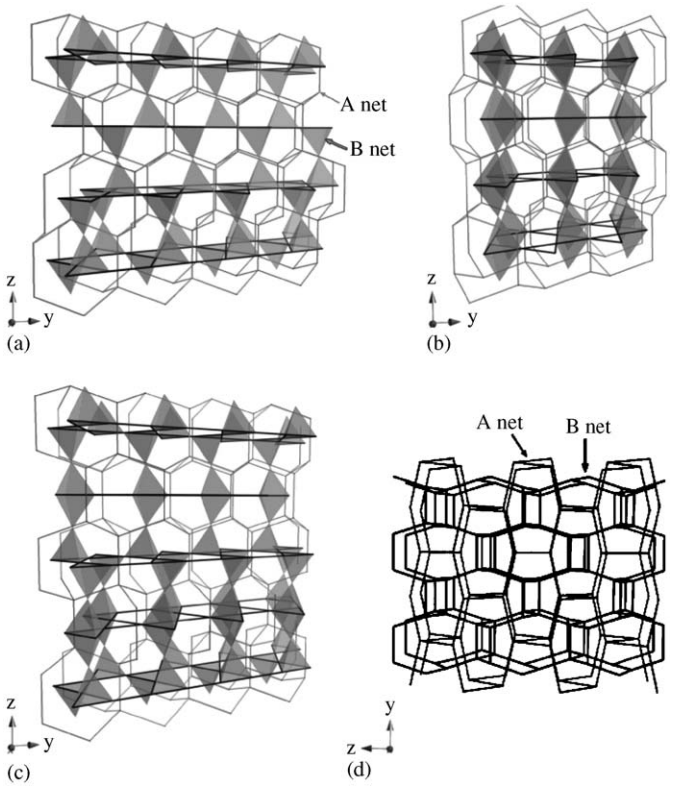

Fig. 1. Structural models of the three primary AB_2 Laves structures, (a) C15 type or $MgCu_2$ type, (b) C14 type or $MgZn_2$ type, (c) C36 type of $MgNi_2$ type, and the KHg_2 ($CeCu_2$) structure (d). The A net is drawn with light grey lines and the B atoms are shown as B_4 tetrahedra. The Kagome net is drawn with solid lines. For clarity, only one Kagome net out of four is shown for the cubic C15 type in (a).

among main group metals allow only very limited combinations of A and B where the radius ratio comes close to that of a topologically close packing ($r_A/r_B = 1.225$). Additionally, the electronegativity of main group metals change significantly from one group to another. With increasing electronegativity difference between the A and B component polar compounds are formed, where typically B atoms form networks (polyanions) with lower coordination numbers compared to Laves phases. One AB_2 example is the KHg_2 ($CeCu_2$) structure type (cf. Fig. 1).

We have previously reported on the pseudobinary systems $AeAl_{2-x}Mg_x$ (Ae = Ca, Sr, Ba) [11,12]. In $CaAl_{2-x}Mg_x$ the sequence of Laves phase structures C15 type→C36 type→C14 type is realised with increasing x (decreasing VEC). The underlying phases have distinct stability ranges in terms of VEC. Very similar ranges are observed in the systems $CaAl_{2-x}Li_x$ [13] and $AeAl_{2-x}Mg_x$ (Ae = Sr, Ba), although size effect prohibits the formation of the $MgCu_2$ type for the latter.

In this work, we extend our investigation of structural and phase stability of *s–p* Laves phases to the system $CaAl_{2-x}Zn_x$. $CaAl_2$ crystallises in the cubic C15 type [14]. The substitution of Al by Zn leads to a slight decrease in the volume per formula unit (V/Z) and to a sizeable increase of polarity because of the larger electronegativity of Zn compared to Al (1.7 and 1.5, respectively, on the Allred–Rochow scale). At a certain concentration x, the Laves phase structure will change into the orthorhombic KHg_2 ($CeCu_2$) structure type, which is adopted by the binary compound $CaZn_2$ [15]. Apparently the KHg_2 type becomes the competing structure to the Laves phase when the ratio r_A/r_B and/or the electronegativity difference between A and B turns too large. The system $CaAl_{2-x}Zn_x$ provides yet another example for the study of VEC-induced Laves phase structural changes, e.g. trivalent Al is replaced by divalent Zn, and one could expect the appearance of additional Laves phases similar to $CaAl_{2-x}Mg_x$ before the transition to the KHg_2-type structure occurs.

2. Experimental

2.1. Synthesis

Polycrystalline samples $CaAl_{2-x}Zn_x$ with $x = 0$, 0.1, 0.15, 0.2, 0.25, 0.3, 0.4, 0.5, 0.6, 0.65, 0.7, 0.8, 0.85, 0.9, 0.95, 1.0, 1.25, 1.5, 1.75, 2.0 were synthesised from the elements (calcium, crystalline dendritic pieces, Alfa Aesar, 99.987%), zinc (shots, Alfa Aesar, 99.9999%) and aluminium (rods, Alfa Aesar, 99.9965%). Calcium pieces, zinc shots and pieces of the aluminium rod were weighed in the appropriate atomic ratios and sealed in tantalum tubes in argon atmosphere. The average mass of a sample for one experiment was 0.5 g. Tantalum tubes were protected from air by a silica jacket sealed under vacuum, heated at 1273 K ($x \geqslant 1.0$) or at 1373 K ($x < 1.0$) for 2 h and subsequently quenched in water. After that samples were directly heated and annealed at 873 K ($x \geqslant 1.0$) for 21 days or at 973 K ($x < 1.0$) for 11 days followed by quenching in water. The silvery grey products could easily be separated as ingots from the tantalum tubes. No visible reaction of the samples with the crucible material could be detected. However, in a few samples chemical analysis revealed traces of Ta. Samples $CaAl_{2-x}Zn_x$ are slightly sensitive to air.

2.2. Characterisation

2.2.1. Chemical analysis

For chemical analysis, the samples were dissolved in concentrated HCl containing a small amount of HF. Chemical analysis was carried out with an ICP Optical Emission Spectrometer (VISTA). Results are given in Table 1. Not all of the samples in the $CaAl_{2-x}Zn_x$ system were single phase, however chemical analysis was conducted to determine the average composition.

2.2.2. Thermal analysis

The thermal behaviour of the $CaAl_{2-x}Zn_x$ samples was investigated by differential thermal analysis (DTA). Data were obtained with a Netzsch DSC 404C setup (thermocouple type S, heating/cooling rate 10 K/min) in argon atmosphere (Messer-Griesheim, 99.999%, additionally

Table 1
Nominal compositions, results from chemical analysis, structure types, lattice parameters for $CaAl_{2-x}Zn_x$

Nominal composition	Composition from chemical analysis	Structure type	Lattice parameters (Å)					
			$MgCu_2$	$MgNi_2$		KHg_2		
			a	*a*	*c*	*a*	*b*	*c*
$CaAl_2$		$MgCu_2$	8.0402(3)					
$CaAl_{1.9}Zn_{0.1}$*	$Ca_{1.00(2)}Al_{1.94(4)}Zn_{0.10(1)}$	$MgCu_2$	8.0341(6)					
$CaAl_{1.85}Zn_{0.15}$*	$Ca_{1.00(4)}Al_{1.88(8)}Zn_{0.15(1)}$	$MgCu_2$	8.0296(3)					
$CaAl_{1.8}Zn_{0.2}$	$Ca_{1.00(1)}Al_{1.80(1)}Zn_{0.20(1)}$	$MgCu_2+MgNi_2$	8.0316(3)	5.6965(4)	18.3803(2)			
$CaAl_{1.75}Zn_{0.25}$*	$Ca_{1.00(1)}Al_{1.78(7)}Zn_{0.25(1)}$	$MgCu_2+MgNi_2$	8.0321(6)	5.6989(2)	18.3796(9)			
$CaAl_{1.7}Zn_{0.3}$*	$Ca_{1.00(1)}Al_{1.79(9)}Zn_{0.30(1)}$	$MgNi_2$		5.6988(3)	18.372(3)			
$CaAl_{1.6}Zn_{0.4}$	$Ca_{1.00(2)}Al_{1.56(3)}Zn_{0.40(1)}$	$MgNi_2$		5.6931(3)	18.3661(3)			
$CaAl_{1.5}Zn_{0.5}$	$Ca_{1.00(2)}Al_{1.47(2)}Zn_{0.50(1)}$	$MgNi_2$		5.6875(4)	18.356(2)			
$CaAl_{1.4}Zn_{0.6}$*	$Ca_{1.00(2)}Al_{1.46(7)}Zn_{0.59(1)}$	$MgNi_2$		5.6816(4)	18.352(3)			
$CaAl_{1.35}Zn_{0.65}$		$MgNi_2$		5.6797(6)	18.348(3)			
$CaAl_{1.3}Zn_{0.7}$	$Ca_{1.00(1)}Al_{1.27(1)}Zn_{0.70(1)}$	$MgNi_2+KHg_2$		5.6776(5)	18.346(2)	4.5662(7)	7.390(1)	7.922(1)
$CaAl_{1.2}Zn_{0.8}$	$Ca_{1.00(1)}Al_{1.17(1)}Zn_{0.80(1)}$	$MgNi_2+KHg_2$		5.6762(3)	18.345(1)	4.5704(5)	7.3902(8)	7.9219(8)
$CaAl_{1.15}Zn_{0.85}$		$MgNi_2+KHg_2$		5.6757(8)	18.345(3)	4.5722(3)	7.3914(7)	7.9236(9)
$CaAl_{1.1}Zn_{0.9}$	$Ca_{1.00(1)}Al_{1.08(1)}Zn_{0.92(1)}$	$MgNi_2+KHg_2$		5.675(2)	18.345(9)	4.5666(6)	7.3901(7)	7.9179(4)
$CaAl_{1.05}Zn_{0.95}$		KHg_2				4.5710(3)	7.3835(5)	7.9231(6)
$CaAl_{1.0}Zn_{1.0}$	$Ca_{1.00(1)}Al_{0.98(1)}Zn_{1.01(1)}$	KHg_2				4.5675(4)	7.3750(5)	7.9224(4)
$CaAl_{0.75}Zn_{1.25}$	$Ca_{1.00(1)}Al_{0.73(1)}Zn_{1.30(3)}$	KHg_2				4.5652(6)	7.3672(6)	7.9001(5)
$CaAl_{0.5}Zn_{1.5}$	$Ca_{1.00(1)}Al_{0.49(1)}Zn_{1.54(2)}$	KHg_2				4.5675(2)	7.3654(5)	7.8434(5)
$CaAl_{0.25}Zn_{1.75}$	$Ca_{1.00(3)}Al_{0.24(1)}Zn_{1.81(2)}$	KHg_2				4.5787(2)	7.3725(6)	7.7640(5)
$CaZn_2$		KHg_2				4.5906(3)	7.3819(6)	7.6796(4)

Samples containing traces of Ta are marked with an asterisk.

purified by passing over BTS catalyst, Merck) using sealed niobium ampoules. Melting points of five pure metals were employed for the temperature calibration. The uncertainty of the DTA measurements was estimated to $\pm 3\,^{\circ}C$ for the measurements. Melting temperatures were established as t_{onset} from heating curves. The liquidus was established in the same way except that peak temperatures were used.

2.2.3. Transmission electron microscopy (TEM)

Selected samples $CaAl_{2-x}Zn_x$ were subjected to transmission electron microscope (TEM) investigations (JEOL 2100F operated at 200 kV) in order to obtain complementary information to the X-ray diffraction (XRD) analysis. Supposing the C14 and C36 phases have very similar volumes per formula unit and very similar *a*-axis parameters, the identification of the C14 phase in a possible two-phase region with the C36 phase might be difficult from X-ray powder diffraction data. Therefore, selected area diffraction (SAD) patterns and HRTEM images were acquired. For two-phase samples, compositions of each phase were analysed locally by energy-dispersive X-ray (EDX) analysis. A full TEM analysis including structural changes under strong electron beam irradiation in the $CaAl_{2-x}Zn_x$ system is discussed in Ref. [16].

2.2.4. Powder X-ray diffraction

To evaluate the phase fields and to determine the unit cell dimensions, powder XRD data were collected with a Huber imaging plate (IP) Guinier Camera 670 using Cu$K\alpha_1$ ($\lambda = 1.54056$ Å) radiation. Silicon powder ($a = 5.43119$ Å) was added to the samples as internal standard. Powdered samples were prepared from the ingots by mechanical grinding. The phases in the samples were identified with the PowderCell programme [17] and the cell parameters were refined with the programme PIRUM [18].

High-resolution powder XRD patterns were collected using the Debye–Scherrer camera installed at the SPring-8, BL02B2 beamline, Japan [19]. A monochromatic X-ray beam with $\lambda = 0.40102$ Å was used. Samples with uniform particle size (ca. 10 μm) were prepared by grinding, sieving and precipitation. Subsequently the samples were packed and sealed in glass capillaries with a diameter of 0.2 mm under argon atmosphere. During the measurements the samples were rotated and cooled by a gas flow from liquid nitrogen. Complete diffraction profiles were collected with an IP with a size of $200 \times 400\,mm^2$, and one pixel corresponding to 0.01° in 2θ scattering angle. The highest count of the powder pattern was about 5.0×10^5 counts, which represents the goodness of counting statistics for the present data. The XRD profiles were analysed with the Rietveld refinement programme rwpy906 [20]. Refinements were performed based on the intensity of

$$I(hkl) = \frac{\text{Const}}{\sin 2\theta \sin \theta} |F(hkl) \exp\{-Bs^2(hkl)\}|^2 j_{hkl},$$

where 2θ is the scattering angle, $F(hkl)$ is the structure factor, B is the isotropic displacement parameter, s is equal to $\sin\theta/\lambda$, and j_{hkl} is the multiplicity.

3. Results

3.1. Phase relations in $CaAl_{2-x}Zn_x$

Fig. 2 shows the powder XRD patterns for three representative $CaAl_{2-x}Zn_x$ samples ($x = 0.15$, 0.65, 0.95). From the observed patterns that the C15 type Laves phase (Fig. 2a) exists only in a narrow compositional range of $0 \leqslant x \leqslant 0.18$. The C36 type Laves phase can be observed in the range of $0.28 \leqslant x \leqslant 0.68$ (Fig. 2b). The orthorhombic KHg_2-type phase has the widest compositional range, i.e. $0.93 \leqslant x \leqslant 2.0$ (Fig. 2c). Cell parameters obtained from powder XRD are given in Table 1. Fig. 3 shows how the volume (per 8 formula units $CaAl_{2-x}Zn_x$) depend on the concentration x at room temperature. Along the structural change C15→C36, the volume changes almost monotonically, and the lattice parameters decreases isotropically. In contrast, the transition from the C36 to the KHg_2 structure is accompanied by a volume discontinuity of 4.6%. Most apparent are the anisotropic changes of the lattice parameters of the Zn-rich phase: Whereas a and b alter only slightly with increasing x, the c parameter decreases considerably (cf. Table 1).

TEM investigations were carried out in order to clarify: (i) the nature of the two-phase regions (i.e. the possibility of delicate intergrowth structures from the cubic C15 and hexagonal C36 type or even the occurrence of the C14 type in the region between stable C36 and KHg_2-type phases) and (ii) a possible Al/Zn ordering in the KHg_2 structure, especially for the composition $CaAl_{1.0}Zn_{1.0}$. Fig. 4a shows a HRTEM image taken from the $CaAl_{1.3}Zn_{0.7}$ sample, which is a mixture of the C36 and the KHg_2-type phase. This image can only be interpreted with the C36 structure (the simulated image together with the stacking structural model are displayed on the left-hand side of

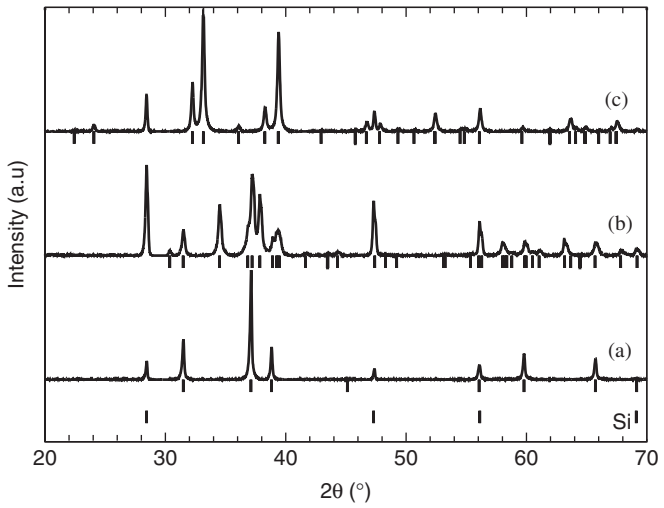

Fig. 2. X-ray diffraction patterns of three representative $CaAl_{2-x}Zn_x$ alloys: (a) $x = 0.15$ (C15 type), (b) $x = 0.65$ (C36 type) and (c) $x = 0.95$ (KHg_2 type). The vertical bars show the calculated Bragg reflection positions and the vertical bars on the bottom show the reflection positions for silicon, which was used as an internal standard.

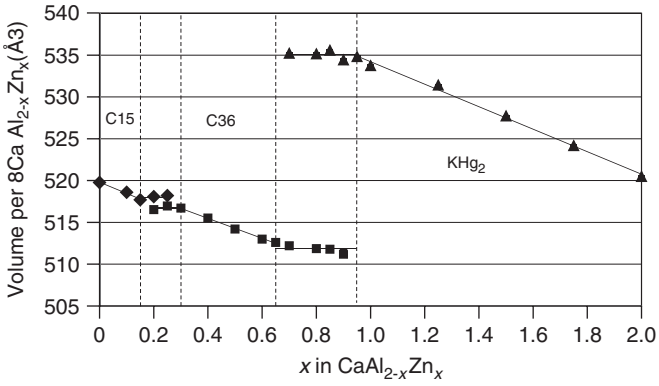

Fig. 3. Volume per eight formula units $CaAl_{2-x}Zn_x$ vs. Zn concentration (x). Error bars are smaller than the size of the symbols.

Fig. 4a). The corresponding electron diffraction (ED) pattern from this sample is shown in Fig. 4b together with simulated ED patterns for the C36 and C14 types. It is important to notice that these two structures—if coexisting—are clearly distinguishable by TEM investigations, whereas the presence of a mixture would have been very difficult to detect by X-ray powder diffraction. We conclude that the C36-type phase is coexisting with the KHg_2-type phase and, thus, a C14-type phase is not present in the $CaAl_{2-x}Zn_x$ system. We further conclude from TEM investigations (not shown here) that the C15–C36 type two-phase region in the $CaAl_{2-x}Zn_x$ system represents a macroscopic mixture where the constituting phases coexist in their corresponding boundary compositions. This is analogous to the $CaAl_{2-x}Mg_x$ system, but in contrast to systems such as $MgNi_{2-x}Cu_x$, $MgCu_{2-x}Zn_x$, or $MgZn_{2-x}Ag_x$, where between the stability ranges of the primary Laves phase structure types, complex polytypes—i.e. microscopic mixtures of the primary structure types—occur [7–10]. No superstructure reflections based on Al/Zn ordering could be observed in the C15-, C36- or KHg_2-type phases. This holds true especially for the composition $CaAl_{1.0}Zn_{1.0}$, which would allow the formation of KHg_2-type subgroup related derivatives (such as the TiNiSi structure with space group *Pnma*) [21]. Firstly, we could not observe any extra reflections in the ED patterns of $CaAl_{1.0}Zn_{1.0}$ crystals, and, secondly, convergent beam electron diffraction (CBED) patterns clearly showed the space group symmetry *Imma* of the KHg_2 type [16].

The pseudobinary $CaAl_2$–$CaZn_2$ phase diagram as sketched from the results of our XRD, DSC and TEM investigations is shown in Fig. 5. $CaAl_2$ has a solid solubility range up to $CaAl_{1.82}Zn_{0.18}$. The phase forms congruently at 1075 °C at $x = 0$. The C36-type intermediate phase has a solid solubility range from $CaAl_{1.72}Zn_{0.28}$ to $CaAl_{1.32}Zn_{0.68}$ and forms peritectically from $CaAl_2$ and the melt at 954 °C. In KHg_2-type $CaZn_2$ about half of the zinc atoms can be exchanged for aluminium. The limiting composition is $CaAl_{1.07}Zn_{0.93}$. The solid solution $CaAl_{2-x}Zn_x$ ($0.93 \leqslant x \leqslant 2$) forms peritectically with an approximate composition $CaAl_{1.05}Zn_{0.95}$ from the

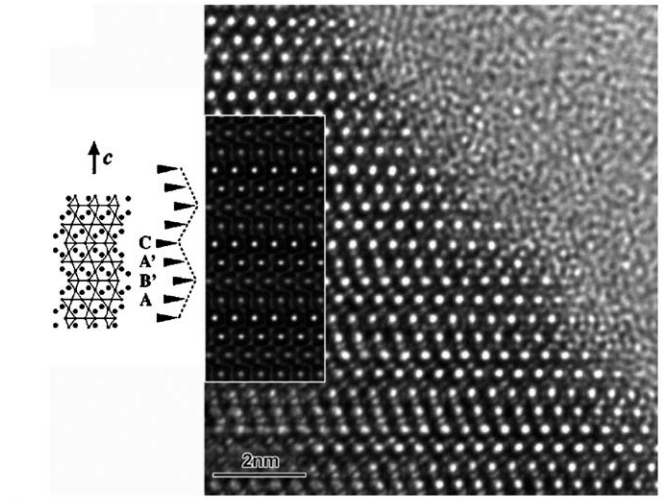

(a)

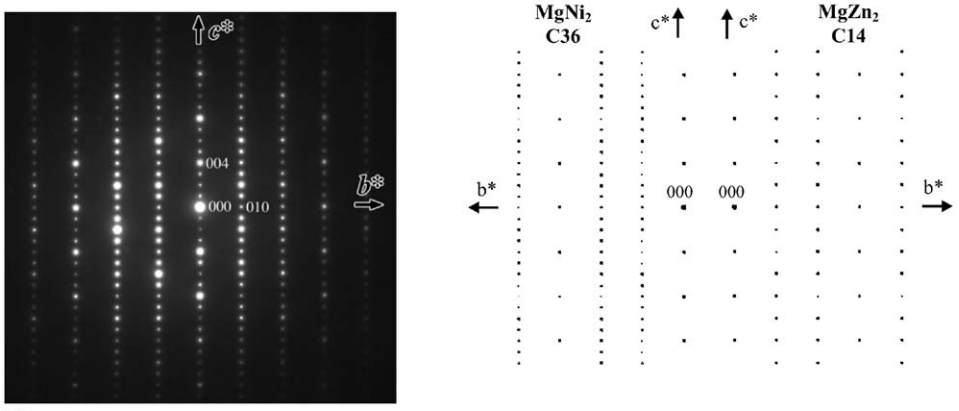

(b)

Fig. 4. (a) HRTEM image of $CaAl_{1.3}Zn_{0.7}$. (b) ED pattern of $CaAl_{1.3}Zn_{0.7}$ along [100], together with simulated patterns for the C36 and C14 structure. Systematic absent reflections (e.g. 001, 002, 003) visible in the ED pattern are due to dynamical diffraction effects. This was confirmed experimentally by tilting the crystal along the *c*-axis.

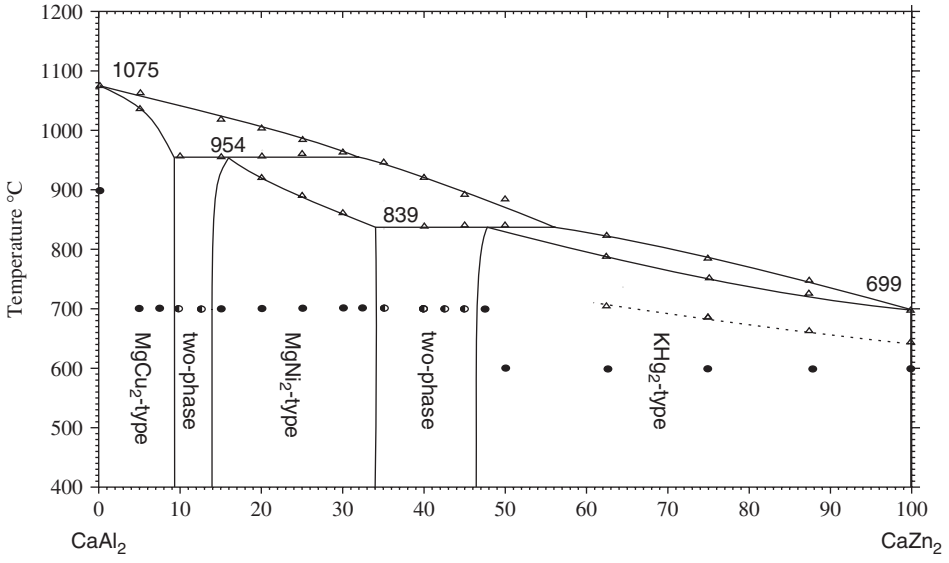

Fig. 5. Sketch of the pseudobinary $CaAl_2$–$CaZn_2$ phase diagram. The broken line is associated with the peritectic formation of impurity $Ca_{3.33}Zn_{10.11-x}Al_x$.

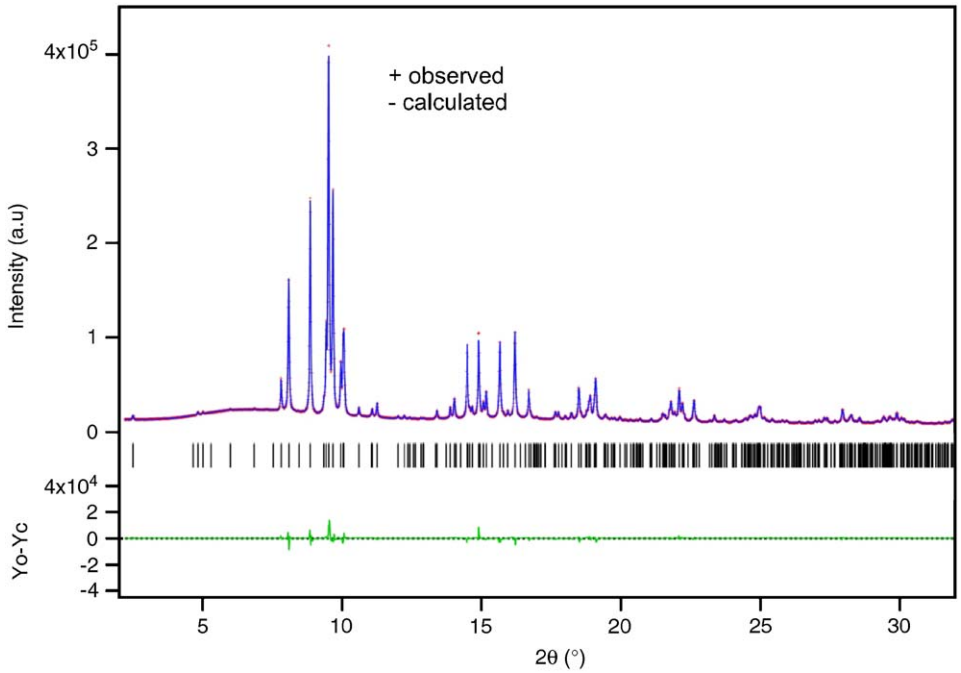

Fig. 6. Observed (+) and calculated powder X-ray diffraction profiles (solid line) of $CaAl_{1.7}Zn_{0.3}$. The Bragg peaks are noted by tic marks below the profile. A difference curve (observed minus calculated data) is shown at the bottom. A background correction has been applied.

C36-type intermediate phase and the melt at 839 °C. Binary $CaZn_2$ forms congruently at a lower temperature (699 °C). Small thermal effects were observed for compositions that were more zinc-rich than $CaAl_{0.75}Zn_{1.25}$ in the range from 705 °C for the composition $CaAl_{0.75}Zn_{1.25}$ to 639 °C for the composition $CaZn_2$. This can be explained with a presence of a small impurity of $Ca_{3.33}Zn_{10.11-x}Al_x$ [22], which has a reported peritectic formation temperature of 642 °C [1].

3.2. Crystal structure refinements

Rietveld refinements were carried out on synchrotron powder diffraction data for five $CaAl_{2-x}Zn_x$ samples: $x = 0.0$, 0.15 (C15) and $x = 0.30$, 0.5, 0.65 (C36). The observed diffraction pattern for $CaAl_{1.7}Zn_{0.3}$ is shown in Fig. 6 together with the difference between the observed and calculated intensity at each step. Atomic coordinates, isotropic displacement parameters and occupancies for $CaAl_{1.7}Zn_{0.3}$ are given in Table 2. The correlation between isotropic displacement parameters and site occupancies was negligible (coefficients were around 0.1). Two important aspects of the C36-type structure are worth mentioning: (i) the site 6h (x, $2x$, $\frac{1}{4}$; site symmetry $mm2$) which forms a flexible Kagome net of B atoms has a tendency to be preferentially occupied by Zn (i.e. the more electronegative atom); and (ii) atomic positions in the Kagome net of the 6h position ($x = 0.1624(2)$, 0.1621(2) and 0.1625(1) for $CaAl_{1.7}Zn_{0.3}$, $CaAl_{1.5}Zn_{0.5}$ and $CaAl_{1.35}Zn_{0.65}$, respectively) deviate from the ideal uniform position ($x = 1/6 \approx 0.1667$). A similar trend in deviation was observed for the C36 phase in the $CaAl_{2-x}Mg_x$ system [11].

Table 2
Atomic coordinates and displacement parameters for C36 $CaAl_{1.7}Zn_{0.3}$, space group $P6_3/mmc$ ($a = 5.68894(2)$ Å and $c = 18.3384(1)$ Å, $T = 80$ K, $R_{wp} = 1.63\%$, $R_i = 1.95\%$)

Atom	Site	x	y	z	B (Å^2)	Occupancy
Ca1	4*e*	0	0	0.40688(4)	0.502(5)	1
Ca2	4*f*	1/3	2/3	0.65573(4)	0.502	1
Al1	4*f*	1/3	2/3	0.37078(4)	0.636(5)	0.8617(9)
Zn1						0.1383
Al2	6*g*	1/2	0	0	0.636	0.8855(7)
Zn2						0.1145
Al3	6*h*	0.1624(2)	2x	1/4	0.636	0.8068(7)
Zn3						0.1932

4. Discussion

The purpose of our discussion is to establish crudely the factors that govern structural stability between Laves phases and KHg_2-type phases. The KHg_2 structure (Fig. 1d) features a three-dimensional four-connected network of B atoms whereas in the Laves phase structures this connectivity is six. This structure is derived from the simple AlB_2 structure by corrugating hexagon layers in the way they appear in black phosphorous and connect them to give a ladder of four-membered rings [23]. The coordination number of A atoms is 12 + 4 as in the Laves phases. However, the arrangement of coordinating atoms has a much lower symmetry and thus provides a much higher flexibility to accommodate large A atoms.

We assembled a simple structure map for *s-p* AB_2 systems (A = Ca, Sr, Ba; B = Zn, Cd, Hg, Mg, Al) based

on the electronegativity [24] difference between the components and the size ratio r_A/r_B, as illustrated in Fig. 7. The size ratio was calculated from the Goldschmidt radii. The map includes results from previous investigations on $Ae Al_{2-x}Mg_x$ (Ae = Sr, Ba) [11,12] and data for $CaZn_{2-x}Cd_x$ [25]. It is especially the pseudobinary systems which give the most valuable input to this map. In the structure map the Laves phase and KHg_2-type compounds become nicely separated. Note that both exist for VECs ranging from 6 to 8 electrons per formula unit. Laves phases segregate in the lower part (low electronegativity difference and lower r_A/r_B ratios) whereas KHg_2 phases accumulate in the upper part (high electronegativity difference and higher r_A/r_B ratios). It is important to note that: (i) size ratio variations for *s–p* Laves phases can be rather large (i.e. the stability argument of optimum space filling of differently sized spheres is rather weak here) and that (ii) especially the charge transfer/polarity (i.e. the electronegativity difference between *A* and *B*) represents the critical stability determining parameter between the Laves and the KHg_2-type phases.

The structural change C15→C36 in $CaAl_{2-x}Zn_x$ is induced by the decrease in VEC. The same transition is observed in the systems $CaAl_{2-x}Mg_x$ and $CaAl_{2-x}Li_x$. In the latter systems the C36 structure is succeeded by a C14 structure at higher concentrations of x, i.e. at even lower VEC. According to Fig. 7 the C36→C14 transition is suppressed in $CaAl_{2-x}Zn_x$ by the too large electronegativity difference between the *A* and *B* components. The origin of the structural trend C15 type→C36 type→C14 type in *s–p* systems upon decreasing the VEC has been explained by the method of moments [26,27]: When going from the $MgCu_2$ to the $MgZn_2$ structure, the concentration of four-membered rings (and thus the fourth moment) in the *B* atom network is successively increased, which stabilises a structure at a lower band filling (i.e. lower values of VEC) [11].

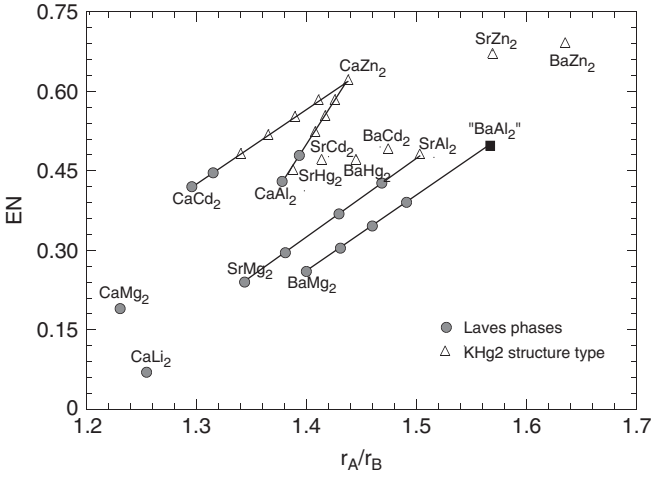

Fig. 7. Structure map for *s–p* AB_2 compounds (A = Ca, Sr, Ba; B = Zn, Cd, Hg, Mg, Al). The parameters are Goldschmidt radius ratio and electronegativity difference. Laves phases are marked with circles and KHg_2-type phases with triangles. $BaAl_2$ does not exist at ambient conditions. The solid lines represent results on $CaAl_{2-x}Zn_x$ (this work), $Ae Al_{2-x}Mg_x$ (Ae = Sr, Ba) [9] and $CaZn_{2-x}Cd_x$ [22].

5. Conclusions

Phase and structural stability relations within the AB_2 pseudo-binary system $CaAl_{2-x}Zn_x$ were studied and yielded a ternary C36-type Laves phase in the compositional range $0.28 \leqslant x \leqslant 0.68$. Rietveld refinement indicated a preferential occupation of Zn on the 6 h position. The C15 Laves phase structure occurs at low zinc concentrations, $0 \leqslant x \leqslant 0.18$. No C14 phase could be observed in this system. Above $x \geqslant 0.93$ the C36 Laves phase structure is succeeded by the KHg_2-type structure which is also the structure of $CaZn_2$. This structural change is explained by the increased electronegativity difference between *A* and *B* component at higher Zn concentrations which favours the formation of polar intermetallic structures where *B* atoms attain lower connectivity.

Acknowledgments

O.T. thanks the Swedish Science Council, VR and the Japan Science Technology Corporation, JST for financial support. U.H. acknowledges support from the Carl Trygger foundation. The authors thank T. Yokosawa and Z. Liu for a part of the TEM investigations, Gudrun Auffermann for chemical analyses, Horst Borrmann, Steffen Hückmann, and Yurii Prots for XRD measurements. The synchrotron radiation experiments were performed at SPring-8 with the approval of the Japan Synchrotron Radiation Research Institute (JASRI). The authors thank Dr. K. Kato of JASRI for his kind help in the experiments.

References

[1] T.B. Massalski (Ed.), Binary Alloy Phase Diagrams, second ed, ASM International, Materials Park, OH, 1990.
[2] F. Laves, Naturwissenschaften 27 (1939) 65.
[3] U. Dehlinger, G.E.R. Schulze, Z. Kristallogr. 102 (1940) 377.
[4] F. Laves, H. Witte, Metall-Wirtsch. Wiss. Tech. 15 (1936) 840.
[5] J. Hafner, J. Phys. F: Met. Phys. 15 (1985) 1879.
[6] F. Stein, M. Palm, G. Sauthoff, Intermetallics 12 (2004) 713.
[7] Y. Komura, A. Nakaue, M. Mitarai, Acta Crystallogr. B 28 (1972) 727.
[8] Y. Komura, M. Mitarai, A. Nakaue, S. Tsujimoto, Acta Crystallogr. B 28 (1972) 976.
[9] Y. Komura, Y. Kitano, Acta Crystallogr. B 33 (1977) 2496.
[10] Y. Komura, K. Tokunaga, Acta Crystallogr. B 36 (1980) 1548.
[11] S. Amerioun, S. Simak, U. Häussermann, Inorg. Chem. 42 (2003) 1467.
[12] S. Amerioun, T. Yokosawa, U. Häussermann, Inorg. Chem. 43 (2004) 4751.
[13] R. Nesper, G.J. Miller, J. Alloys Compds. 197 (1993) 109.
[14] H. Nowotny, A. Mohrnheim, Z. Kristallogr. 100 (1939) 540.
[15] G.E.R. Schulze, J. Wieting, Z. Metallkd. 52 (1961) 743.
[16] T. Yokosawa, K. Söderberg, M. Boström, D. Grüner, G. Kreiner, O. Terasaki, Z. Kristallogr., in press.

[17] W. Kraus, G. Nolze, Federal Institute for Materials Research and Testing, Berlin, Germany, 2000.
[18] P.-E. Werner, Ark. Kemi 31 (1969) 513.
[19] E. Nishibori, M. Takata, K. Kato, M. Sakata, Y. Kubota, S. Aoyagi, Y. Kuroiwa, M. Yamakata, N. Ikeda, Nucl. Instrum. Methods A 467–468 (2001) 1045–1048.
[20] Y. Kubota, Program for Rietveld Analysis, rwpy906, 2005.
[21] R.-D. Hoffmann, R. Pöttgen, Z. Kristallogr. 216 (2002) 127.
[22] M.L. Fornasini, F. Merlo, Acta Crystallogr. B38 (1980) 1739.
[23] G. Nuspl, K. Polborn, J. Evers, G.A. Landrum, R. Hoffmann, Inorg. Chem. 35 (1996) 6922.
[24] A.L. Allred, E.G. Rochow, J. Inorg. Nucl. Chem. 5 (1958) 264.
[25] E.-L. Nordmark, U. Häussermann, (2000), unpublished results.
[26] D.G. Pettifor, Bonding and Structure of Molecules and Solids, Clarendon Press, Oxford, UK, 1995.
[27] J.K. Burdett, S. Lee, J. Am. Chem. Soc. 107 (1985) 3050.